Temperature and magnetic field dependence of the induced magnetization in macroscopic samples due to the proximity effect

Yu. N. Ovchinnikov and B. I. Ivlev
L. D. Landau Institute for Theoretical Physics, Russian Academy of Sciences, Kosygin 2, Moscow, 11733V, Russia

R. J. Soulen, Jr. and J. H. Claassen
Naval Research Laboratory, Code 6344, Washington, D.C. 20375-5000

W. E. Fogle
Materials Sciences Division, Lawrence Berkeley Laboratory, Berkeley, California 94720

J. H. Colwell*
National Institute of Standards and Technology, Gaithersburg, Maryland 20899
(Received 31 March 1997)

We have applied the Ginzburg-Landau equations to calculate the behavior of the diamagnetism of macroscopic samples consisting of a normal metal in contact with a superconductor. In particular, the calculation focuses on the temperature region above the superconductive transition temperature T_{cN} of the normal metal. We have compared these calculations with experimental measurements of the temperature (0.006–1 K) and magnetic field (10^{-9}–10^{-6} T) dependence of the diamgnetism for several samples of Be ($T_{cN}\sim 23$ mK) and W ($T_{cN}\sim 15.5$ mK) in contact with the superconductor Al ($T_{cS}=1.18$ K). The agreement between the predictions and measurements is quite good and confirms the approach of using the Ginzburg-Landau model to calculate the proximity effect in macroscopic normal systems above their superconductive transitions. [S0163-1829(97)03738-7]

I. INTRODUCTION

The ramifications of the proximity effect have been studied experimentally by measuring the electrical resistance of normal/superconducting (N/S) interfaces,[1] by measuring the critical current of $S/N/S'$ trilayers,[2,3] by measuring the kinetic inductance of S/N bilayers,[4] and by measuring the diamagnetism of N/S bilayers[5] and S cylinders sheathed by N metal.[6–9] The data have been generally interpreted within the theoretical framework of the Ginzburg-Landau (GL) equations[10] or the de Gennes–Werthamer formulation.[11]

In the diamagnetic case, the applied magnetic field is partially shielded from the interior of the N material and the detected signal is proportional to the product of the diamagnetic susceptibility $\chi=-1/4\pi$ and the excluded volume. For a cylindrical geometry the diamagnetic signal is proportional to x_0, which is the effective radius that magnetic fields are excluded from the normal metal. The parameter x_0 is governed by the behavior of the coherence length ξ_N in the normal metal and by $\lambda(0)$, the value of the penetration depth at the N/S interface. When $\xi_N \gg \lambda(0)$ and when the applied magnetic field is less than $H_0=\phi_0/2\pi\xi_N^2$, then x_0 is given by[12]

$$x_0=\xi_N\{\ln[\xi_N/\lambda(0)]-0.116\}, \tag{1}$$

where $\phi_0=\pi\hbar c/e$ is the flux quantum. Equation (1) indicates that x_0 is independent of magnetic field. Its temperature dependence is given implicitly by ξ_N. In the two extreme limits of sample purity, this quantity is given by

$$\xi_N=\hbar v_F/2\pi k_B T \quad \text{(clean limit)}$$
$$=(\hbar v_F l/6\pi k_B T)^{1/2} \quad \text{(dirty limit)}, \tag{2}$$

where v_F is the Fermi velocity of the normal metal, k_B is Boltzmann's constant, l is the mean free path in the normal metal, and T is the temperature. The respective temperature behavior for the two limits can be shown to be a consequence of the fact that a transition between them occurs when $l=\hbar v_F k_B T/2\pi$ [see Eqs. (6) and (7) which follow]. Since the induced diamagnetism δM is proportional to $\xi_N \ln \xi_N$, it is clear that its predominant temperature dependence is determined by the behavior of ξ_N.

One group[6,7] did observe that the diamagnetism of Nb cylinders sheathed by impure Cu or Au was proportional to $T^{-1/2}$, thereby confirming the prediction for the dirty limit. In cleaner materials, however, there is less consensus: One group[8] found that $\delta M \alpha T^{-1.5}$ for Nb/Cu samples and that $\delta M \alpha T^{-2}$ for Nb/Ag samples. A second group[9] found that several different power laws were necessary to describe the behavior of different samples of Nb and NbTi encased in clean Cu. A possible explanation for the considerable variation in the clean limit has been proposed by Belzig *et al.*[13] They solved the GL equations numerically and confirmed the $T^{-1/2}$ dependence for the impure limit, but obtained a stronger temperature behavior for the diamagnetism (roughly exponential) in the clean limit. Thus the diamagnetism of samples of slightly differing impurity near the pure limit might be characterized by a wide variation in the exponent of temperature. This conjecture, however, has not been submitted to a quantitative study.

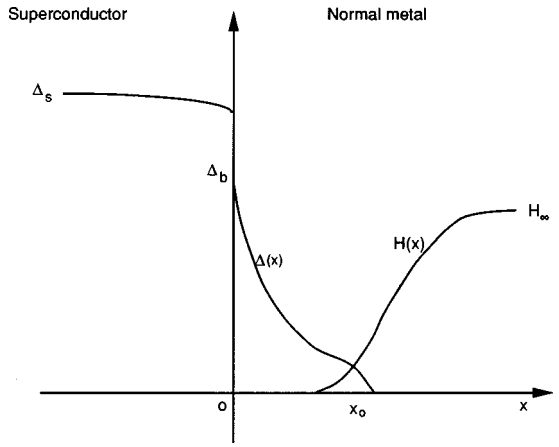

FIG. 1. Schematic representation of the spatial dependence of the order parameter and magnetic field for a semi-infinite interface between a superconductor S and normal metal N.

When $H>H_0$, the diamagnetism retains the same temperature dependence, but takes on a magnetic field dependence, which has also been calculated.[12] The expression for x_0 is given by

$$\sinh(x_0/\xi_N)=\phi_0/2\pi\lambda(0)\xi_N H. \tag{3}$$

There has been no systematic study of the magnetic field dependence of δM, although in Ref. 7 it was reported that the diamagnetism of two samples varied as $-\ln H$ [a limit of Eq. (3)].

T_{cN} was considered to be zero in the theoretical treatment used above to calculate $\delta M(H,T)$. Furthermore, the samples studied were composed of normal metals (e.g., Cu, Ag) for which this condition was clearly satisfied. In this paper we consider the case for which the normal metal has a finite superconductive transition temperature T_{cN} and we present a calculation of the temperature and magnetic field dependence of the diamagnetism in the temperature range just above T_{cN}. These predictions differ somewhat from those for the case when $T_{cN}\sim 0$. We have carried out measurements of the diamagnetism of several materials with finite T_{cN} over a wide range of temperature and magnetic field and compared the results with these predictions.

II. THEORY

A. Ginzburg-Landau equations and the induced diamagnetism

We consider a macroscopic sample consisting of a normal metal N in intimate contact with a superconductor S. A magnetic field is applied parallel to the interface between the two (Fig. 1). The problem of screening the magnetic field from the interior of the normal metal can be treated as one dimensional, in which case the idealized planar geometry depicted in Fig. 1 and Fig. 3(a) applies. Depending on the magnitude of the superconductive order parameter Δ in the normal metal, two different regimes are possible. When Δ is very small, the magnetic field is not appreciably screened in the normal metal near the N/S interface, whereas when Δ is larger, screening of the magnetic field occurs over a distance on the order of the coherence length in the normal metal and it is readily observed as a change in the diamagnetism.[6,7]

The second case (significant screening in the normal metal) is the more interesting one, which will be considered here. The additional diamagnetization δM is defined by the expression

$$\delta M=\frac{S_A}{4\pi}\int_0^\infty dx[H_\infty-H(x)], \tag{4}$$

where S_A is the surface area of the N/S interface and H_∞ is the magnetic field far from the interface ($x\to\infty$). The spatial dependence of the magnetic field and modulus of the order parameter are represented schematically in Fig. 1.

Near the critical temperature T_{cN}, the magnetic field and the order parameter in the normal metal are described by the Ginzburg-Landau equations

$$-(\mathrm{sgn}\tau)\xi_N^2\left[\frac{\partial^2\Delta}{\partial x^2}-\left(\frac{2\pi}{\phi_0}\right)^2A^2\Delta\right]=\left(1-\frac{7\zeta(3)}{8\pi^2\tau}\frac{\Delta^2}{k_B^2T^2}\right)\Delta, \tag{5}$$

$$j=\left(-\frac{\pi ne^2\eta}{2mc}\frac{\Delta^2}{k_B^2T^2}\right)A,\quad \frac{4\pi}{c}j=-\frac{\partial^2A}{\partial x^2}, \tag{6}$$

where A is the vector potential, Δ is the modulus of the order parameter, n is the number of electrons per unit volume, p_F is the Fermi momentum, $\tau=(T_{cN}-T)/T_{cN}$, $n=(P_F/\hbar)^3(1/3\pi^2)$, and $\xi_N=\sqrt{\pi\eta\hbar^2v_F^2/24|\tau|k_B^2T^2}$. The quantity η depends on the elastic scattering time τ_{tr} in the normal metal and is given explicitly by

$$\eta=\frac{k_BT\tau_{\mathrm{tr}}}{\hbar}\left[1-\frac{8k_BT\tau_{\mathrm{tr}}}{\hbar\pi}\left\{\Psi\left(\frac{1}{2}+\frac{\hbar}{4\pi k_BT\tau_{\mathrm{tr}}}\right)-\Psi\left(\frac{1}{2}\right)\right\}\right]$$

$$=\frac{k_BT\tau_{\mathrm{tr}}}{\hbar}\quad\text{when}\quad\frac{2\pi k_BT\tau_{\mathrm{tr}}}{\hbar}\ll 1\quad(\text{dirty limit})$$

$$=\frac{7\zeta(3)}{2\pi^3}\quad\text{when}\quad\frac{2\pi k_BT\tau_{\mathrm{tr}}}{\hbar}\gg 1\quad(\text{clean limit}), \tag{7}$$

where Ψ is the digamma function (logarithmic derivative of the Γ function) and ζ is the Riemann zeta function. Equations (5)–(7) are equivalent to Werthamer's formulation of the Ginzburg-Landau equations.[14] The major difference between the calculation to be presented here and those found elsewhere is that in this case T_{cN} is considered to be finite so that, in the temperature region above T_{cN}, the coherence length ξ_N has a singularity at T_{cN} which dominates the temperature dependence of the diamagnetism. For the situation considered in most other treatments ($T_{cN}\sim 0$), ξ_N has the more familiar temperature dependence given by Eq. (2) where the divergence occurs at $T=0$.

Further consideration of these equations depends on the magnitude of the applied magnetic field compared to the field H_0, which is defined as [the basis for this definition will be clear after Eq. (23) is presented]

$$H_0=\frac{48}{\pi}e^{-\gamma}\left(\frac{ck_B^2T^2|\tau|}{e\hbar v_F^2\eta}\right)=\frac{2\phi_0e^{-\gamma}}{\pi\xi_N^2}, \tag{8}$$

where $\gamma=0.577...$ is Euler's constant. Estimates of H_0 for the samples to be reported here indicate that it is on the order of 0.1 μT.

B. Solution for finite T_{cN} in the low-field limit ($H<H_0$)

In the low-field case, where $H<H_0$, the depression of the order parameter by the magnetic field can be neglected even in the important region near x_0 where the magnetic field is screened. Far from the boundary, where Δ is small, the term proportional to Δ^2 may be neglected, in which case the solution to Eq. (5) is

$$\Delta(x)=\Delta_b\exp(-x/\xi_N). \tag{9}$$

Note that τ is negative in the normal metal; the value of the order parameter at the S/N interface, Δ_b, can be found by solving the boundary condition problem (see below).

When Eq. (9) is substituted into Eq. (6), the solution for the vector potential is

$$A=H_\infty\xi_N K_0\left[\frac{\Delta_b e\hbar v_F\eta}{ck_B^2T^2}\sqrt{\frac{\pi^3 n}{12m|\tau|}}\exp(-x/\xi_N)\right], \tag{10}$$

where K_0 is the modified Bessel function. Using the fact that $H=\partial A/\partial x$ and substituting Eq. (10) into Eq. (4), the excess diamagnetization is found to be

$$\delta M=\frac{SH_\infty}{4\pi}x_0=\frac{SH_\infty}{4\pi}\xi_N\left[\ln\left(\frac{\Delta_b e\hbar v_F\eta}{2ck_B^2T^2}\sqrt{\frac{\pi^3 n}{12m|\tau|}}\right)+\gamma\right]. \tag{11}$$

In this weak-field limit ($H<H_0$), x_0 does not depend on magnetic field. The prediction given in Eq. (11) is equivalent to that given by the Superconductivity Group at Orsay [Eq. (1)] if the definition $\lambda(0)^{-2}=2\pi^2 ne^2\eta\Delta_b^2/mc^2k_B^2T^2$ is used.

Having derived these results for x_0, it is important to reconsider a point. Near the interface the term proportional to Δ^2 in Eq. (5) may not be neglected, and so the solution in this case is

$$\Delta(x)=\left(\frac{16\pi^2k_B^2T^2|\tau|}{7\zeta(3)}\right)^{1/2}\Big/\sinh[(x+\hat{x}_0)/\xi_N]. \tag{12}$$

The quantity x_0 is related to Δ_b by the equation

$$\hat{x}_0=\xi_N\ln\left[\sqrt{\frac{16\pi^2k_B^2T^2|\tau|}{7\zeta(3)\Delta_b^2}}+\sqrt{1+\frac{16\pi^2k_B^2T^2|\tau|}{7\zeta(3)\Delta_b^2}}\right]. \tag{13}$$

That is, in the range $x\gg\xi_N$, we obtain

$$\Delta(x)=\frac{2\Delta_b}{1+\sqrt{1+7\zeta(3)\Delta_b^2/16\pi^2k_B^2T^2|\tau|}}\exp(-x/\xi_N), \tag{14}$$

where $\Delta_b=\Delta(+0)$. The effect of this analysis is that the expression for H_0 [Eq. (8)] is to be replaced by the more accurate result

$$H_0=\frac{24}{\pi}e^{-\gamma}\left(\frac{ck_B^2T^2|\tau|}{e\hbar v_F^2\eta}\right)\left[1+\sqrt{1+\frac{7\zeta(3)\Delta_b^2}{16\pi^2k_B^2T^2|\tau|}}\right]. \tag{15}$$

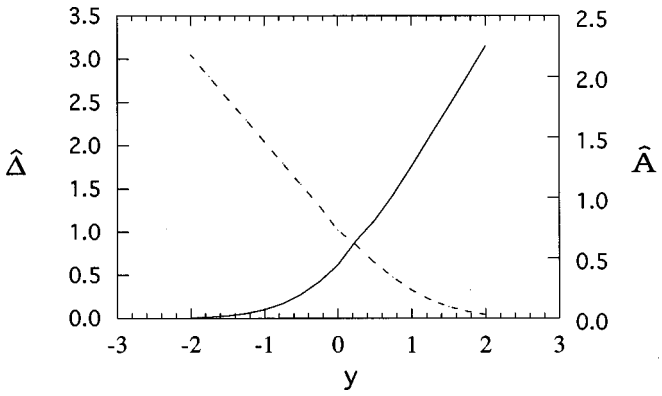

FIG. 2. Spatial variation of the order parameter and vector potential for conditions for which the influence of the magnetic field could not be neglected in solutions for the Ginzburg Landau equations.

C. Solution for finite T_{cN} in the higher-field limit ($H>H_0$)

In the case of a stronger magnetic field, the depression of the order parameter by the field cannot be neglected. At fields $H\gg H_0$, the magnetic field screening and order parameter depression occur at distance of order $(2eH_\infty/c\hbar)^{-1/2}$ near x_0. At such a field, in the vicinity of x_0, the right side of Eq. (5) can be omitted. If we define new dimensionless variables

$$y=(x-x_0)\left(\frac{2eH_\infty}{c\hbar}\right)^{1/2},$$

$$\hat{A}=A\left(\frac{2e}{H_\infty c\hbar}\right)^{1/2},$$

$$\hat{\Delta}=\Delta\left(\frac{mck_B^2T^2H_\infty}{\pi^2n\hbar e\eta}\right)^{-1/2}, \tag{16}$$

Eqs. (5) and (6) become

$$\frac{\partial^2\hat{\Delta}}{\partial y^2}=\hat{A}^2\hat{\Delta},\quad \frac{\partial^2\hat{A}}{\partial y^2}=\hat{\Delta}^2\hat{A}, \tag{17}$$

with boundary conditions $\hat{A}\to y$ and $\hat{\Delta}\to 0$ at $y=+\infty$. The coefficient for $\hat{\Delta}$ can be determined from a numerical calculation in the asymptotic expansion at $y\to+\infty$:

$$\hat{\Delta}=\frac{0.87}{\sqrt{y}}\exp\left(-\frac{y^2}{2}\right). \tag{18}$$

At $y\to-\infty$, $\hat{A}\to 0$, and thus by the symmetry of $\hat{A}$ and $\hat{\Delta}$ in Eq. (17), formally, $\hat{\Delta}\to -y$. The numerical solution of Eq. (17) with the boundary conditions given above is plotted in Fig. 2.

The solution of Eq. (17) should be matched with the solution of the Ginzburg-Landau equation in the region $x<x_0$ where the magnetic field is screened [Eq. (19)]:

$$\Delta(x)=-2\Delta_b\exp(-x_0/\xi_N)\sinh[(x-x_0)/\xi_N]. \tag{19}$$

Matching the solution given in Eq. (19) with the solution of Eq. (17) at $y\to-\infty$ gives the result

$$\Delta = -(x-x_0)\sqrt{\frac{2mk_B^2T^2}{\pi^2 n\eta}}\frac{H_\infty}{\hbar}. \tag{20}$$

We obtain the expression for x_0:

$$x_0 = \xi_N \ln\left[\frac{4\Delta_b}{\hbar H_\infty}\sqrt{\frac{mp_F|\tau|}{\pi\hbar}}\right]. \tag{21}$$

The solutions of the GL equations by the Orsay Group on Superconductivity[12] for finite H and for $T_{cN}=0$ were given previously as a sinh function [Eq. (3)]: Using the approximation $\sinh^{-1}(x)\sim\ln(x)$, we can express that result in a form similar to Eq. (21). It is important to remember, however, that the temperature dependence for ξ_N is different in the two cases.

The expression given in Eq. (21) is valid as long as x_0 is larger than the coherence length in the normal metal. This condition is equivalent to constraining the magnetic field to be less than H_1 where

$$H<H_1=\frac{\Delta_b}{\hbar}\sqrt{\frac{mp_F|\tau|}{\hbar}}=\frac{\Delta_b}{\hbar}\,m\sqrt{\frac{v_F|\tau|}{\hbar}}. \tag{22}$$

An estimate of the ratio of H_1/H_0 (for our samples, $H_1\sim 1.0$ mT) indicates that the magnetic field region extending from H_0 to H_1 should be sufficiently large to allow measurement. Thus we expect the following behavior for $\delta M(H)$: It is independent of magnetic field below H_0 and decreases as $-\ln H$ for $H_0<H<H_1$. For magnetic fields far above H_1, the logarithmic dependence saturates.

An interpolation formula can be written which includes Eqs. (11) and (21) as limiting cases:

$$x_0 = \xi_N \ln\left[\frac{4\Delta_b}{\hbar\sqrt{H_\infty^2+H_0^2}}\sqrt{\frac{mp_F|\tau|}{\pi\hbar}}\right]. \tag{23}$$

Requiring that Eq. (23) match Eq. (11) in the limit $H_\infty\to 0$ defines H_0 given in Eqs. (8) and (15).

D. Calculation of Δ_b

The remaining problem to consider is calculation of Δ_b which appears in the expressions for x_0. In the simpler case where the critical temperature of the metals are close to each other, the Ginzburg-Landau equation is valid everywhere including the boundary region. In this case, it has the form[15]

$$\frac{\pi\hbar^2}{24k_B^2T^2g(x)}\frac{\partial}{\partial x}\left(g(x)v_F^2\eta\frac{\partial\Delta}{\partial x}\right) + \left(1-\frac{T}{T_c(x)}-\frac{7\zeta(3)}{8\pi^2}\frac{\Delta^2}{k_B^2T^2}\right)\Delta = 0, \tag{24}$$

where $g(x)=mp_F/2\pi\hbar^3$ is the density of states evaluated at the Fermi level. Solving this equation and matching $\Delta(0)$ and $\partial\Delta(0)/\partial x$, we find

$$\Delta_b = \sqrt{\frac{16\pi^2k_B^2T^2|\tau|}{7\zeta(3)}}\,z, \tag{25}$$

$$z^2=\frac{\tau_s^2}{2|\tau|}\left[\frac{(p^4\eta)_N}{(p^4\eta)_s}|\tau|+\tau_s + \sqrt{\left(\frac{(p^4\eta)_N}{(p^4\eta)_s}|\tau|+\tau_s\right)^2+\tau_s^2\left(\frac{(p^4\eta)_N}{(p^4\eta)_s}-1\right)}\right]^{-1}, \tag{26}$$

where $\tau_s=1-T/T_{cS}>0$. The index N or S denotes the appropriate metal. If the properties of the metals are approximately identical, that is, $[(p^4\eta)_N\sim(p^4\eta)_S]$, then

$$z^2=\frac{\tau_s^2}{4|\tau|(\tau_s+|\tau|)}. \tag{27}$$

If the temperature is not close to T_{cN}, then Eq. (27) is valid only qualitatively. Note that the $x_0>\xi$ limitation can be easily avoided. For the conditions under consideration, the vector potential may be neglected in Eq. (5) and the Ginzburg-Landau equation has the first integral:

$$-\xi_N^2\left(\frac{\partial\Delta}{\partial x}\right)^2+\Delta^2+\frac{7\zeta(3)}{16\pi^2|\tau|}\frac{\Delta^4}{k_B^2T^2}=\text{const.} \tag{28}$$

With the boundary conditions in the normal metal, $\Delta(x_0)=0$ and $\partial\Delta(x_0)/\partial x=-H_\infty/\hbar\sqrt{2mk_B^2T^2/\pi^2n\eta}$, we find that the value of the constant in Eq. (28) is $-\pi\hbar^3H_\infty^2/4mp_F|\tau|$. Under these conditions, we obtain

$$(x_0-x)\sqrt{\frac{24k_B^2T^2}{\pi\hbar^2v_F^2\eta}}=\int_0^{\Delta(x)}\frac{d\Delta}{\sqrt{\pi H_\infty^2\hbar^3/4mp_F+|\tau|\Delta^2+7\zeta(3)\Delta^4/16\pi^2k_B^2T^2}}. \tag{29}$$

The value of x_0 is determined by the boundary condition at $x=0$. When the critical temperature of the superconductor is also near T_{cN}, then this boundary condition can be easily specified and follows from Eq. (20). The result has the form

$$x_0=\sqrt{\frac{\pi\hbar^2v_F^2\eta}{24k_B^2T^2}}\int_0^{\Delta_b}\frac{d\Delta}{\sqrt{\pi H_\infty^2\hbar^3/4mp_F+|\tau|\Delta^2+\dfrac{7\zeta(3)\Delta^4}{16\pi^2k_B^2T^2}}}, \tag{30}$$

where the order parameter value Δ_b on the N/S boundary is determined by

$$\Delta_b=\frac{\left[\tau_s^2-\frac{H_\infty^2\hbar^3 7\zeta(3)(p^4\eta)_N}{(mp)_N 16\pi k_B^2T^2(p^4\eta)_S}\right]^{1/2}\left(\frac{8\pi^2k_B^2T^2}{7\zeta(3)}\right)^{1/2}}{\left[\tau_S+|\tau|\frac{(p^4\eta)_N}{(p^4\eta)_S}+\sqrt{\left(\tau_S+|\tau|\frac{(p^4\eta)_N}{(p^4\eta)_S}\right)^2+\left(\tau_s^2-\frac{H_\infty^2\hbar^3 7\zeta(3)(p^4\eta)_N}{(mp)_N 16\pi k_B^2T^2(p^4\eta)_S}\right)\left(\frac{(p^4\eta)_N}{(p^4\eta)_S}-1\right)}\right]^{1/2}}. \tag{31}$$

At $H<H_1$ formulas (30) and (31) give the same result as the previous expressions (21)–(25).

E. Solution for $T_{cN}\sim 0$ at low and moderate magnetic fields

The previous expressions derived in this section were appropriate for a sample with a finite T_{cN} and for the temperature region just above that transition, i.e., when $|T-T_{cN}| \ll T_{cN}$. An approximate expression for the magnetization can also be obtained with logarithmic accuracy at temperatures farther from T_{cN} or, equivalently, for a material at finite temperatures and for which $T_{cN}\to 0$. When $T>T_{cN}$ and at large distances from the NS boundary, the order parameter $\Delta(x)$ can be written in the form[16]

$$\Delta(x)=\Delta_b\exp(-k_Nx), \tag{32}$$

where k_N is the smallest root of the equation

$$1+\frac{gmp_F}{2\pi^2}\left[\ln\left(\frac{2e^\gamma\omega_D}{\pi T}\right)+\Psi\left(\frac{1}{2}\right)-\Psi\left(\frac{1}{2}-\frac{k_N^2\eta\hbar^2v_F^2}{12\pi k_B^2T^2}\right)\right]=0. \tag{33}$$

Here g is the electron-phonon coupling constant and ω_D is the Debeye frequency. Equation (33) applies for a normal metal ($g>0$) as well as for a superconductor ($g<0$). As $g\to 0$ or as $T\gg T_{cN}$, Eq. (33) requires that Ψ have a pole. The smallest occurs for the argument to be zero, in which case we obtain $\xi_N=1/k_N=\sqrt{\eta\hbar^2v_F^2/6\pi k_B^2T^2}$. This expression gives the familiar results in the clean and dirty limits, respectively, of $\xi=\sqrt{7\zeta(3)/3}\hbar v_F/2\pi^2k_BT$ and $\xi=\sqrt{\hbar v_Fl/6\pi k_BT}$.

For the superconducting case ($g<0$), the identity $1=(|g|mp_F/2\pi)\ln(2\gamma\omega_D/\pi T_{cN})$ applies and Eq. (33) reduces to

$$-\ln\left(\frac{T_{cN}}{T}\right)=\left\{\Psi\left(\frac{1}{2}-\frac{k_N^2\eta\hbar^2v_F^2}{12\pi k_B^2T^2}\right)-\Psi\left(\frac{1}{2}\right)\right\}. \tag{34}$$

It follows from Eq. (34) that the value x_0 is given with logarithmic accuracy as

$$x_0=k_N^{-1}\ln\left[\frac{k_N\Delta_b}{\hbar\sqrt{H_\infty^2+H_0^2}}\sqrt{\frac{2p_F^2\hbar v_F\eta}{3k_B^2T^2}}\right]. \tag{35}$$

III. EXPERIMENT: DESCRIPTION OF THE APPARATUS AND MEASUREMENT PROCEDURES

The cryogenic apparatus used for these experiments has been described in detail elsewhere.[17] Briefly summarized, it consisted of a ^{3}He-^{4}He dilution refrigerator located inside a radio-frequency-shielded cage. Two high-permeability cylindrical magnetic shields (μ-metal at room temperature and Cryoperm[18] at 4 K) reduced all components of the dc magnetic field at the sample to less than 0.1 μT.[19] The bottom of the mixing chamber of the refrigerator was tailored to accept several thermometers and special holders for the samples. Extensive use of gold-plated copper surfaces promoted good thermal contact among the thermometers and the samples over the operating range of the refrigerator (0.006–2.0 K). The temperature scale[20] used in these measurements is based on NBS-CTS-2, which has an estimated inaccuracy of less than 0.3%. Several resistance thermometers were calibrated versus this temperature scale and were used for measurement of the temperature of the samples.

Three possible sample geometries appropriate for study of the diamagnetism are shown in Fig. 3. The semi-infinite plane shown in Fig. 3(a) is the closest realization of the geometry consistent with the theoretical results shown in Fig. 1, but it was not practical for the samples studied here. The geometry shown in Fig. 3(b), in which an outer N sheath was swaged around the S core, was used in Refs. 6–9. Samples thus formed, however, suffer from compromised purity. For example, the N metals in the studies reported above were inevitably polycrystalline and their residual resistivity ratio (RRR) was at most 1000. The geometry shown in Fig. 3(c), in which the upper end of a single-crystal N material was coated with a superconductor, was used in this study. This configuration was easy to produce, and it offered the additional advantage that it permitted the study of purer samples. Single and polycrystalline samples of Be and W with T_{cN} values of 22.5 and 15.4 mK, respectively, and with RRR values, in some cases in excess of 10 000, were studied. Many of these Be and W samples were also incorporated into National Bureau of Standards Standard Reference Materials 768 superconducting fixed-point devices.[21]

Two or three small spot welds of Al ($T_{cS}\sim 1.18$ K) were

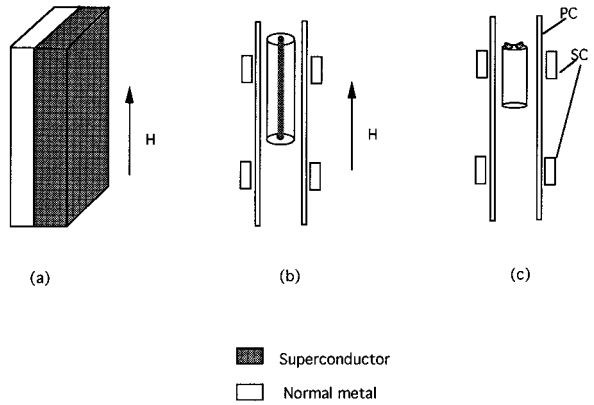

FIG. 3. Three S/N interfaces: (a) semi-infinite plane, (b) cylindrical S enclosed in outer N sheath, and (c) small S spot welded to long N cylinder.

made to the upper end of the sample to serve as the source of superconductivity for the proximity effect. The Al spot welds were applied to one end of each sample by charging a 4-μF capacitor to 30 V and discharging it through a 0.25-mm-diam Al wire in contact to the sample. The Al welds were thus hemispheres roughly 0.25 mm in diameter. Al is a good choice for the source of the proximity effect in the two materials studied in this article since its solubility in them is very small.[22]

Each sample was enclosed in a set of copper coils as shown in Fig. 3(c) in which a long primary coil (PC) was surrounded by a pair of series-opposed secondary coils (SC). The primary coil was considerably longer than the sample and was driven by the oscillator output of a phase-sensitive detector at a frequency f of 1 kHz. Thus the PC produced an ac magnetic field $H(t)=H_{\rm rms}\sin(2\pi ft)$. The amplitude of the oscillator and thus $H_{\rm rms}$ could be adjusted. The induced magnetization due to the sample's response to the applied ac magnetic field was detected by the secondary coil, which was either centered on or near the S material where the proximity effect was expected. A signal proportional to the diamagnetization was measured with an ac mutual inductance bridge of conventional design and construction.[23] A dc magnetic field could also be applied to the sample by injecting a dc current into the primary coil or into a separate coil surrounding the samples.

According to Lenz's law, the voltage induced in the secondary coil, V_S, in response to a magnetic field generated in the primary coil is given by $V_S=M_{12}d\Phi/dt$, where M_{12} is the mutual inductance between the two coils and Φ is the magnetic flux linking them. Using standard electromagnetic relations, it may be shown that $V_S=k_{12}Hf\chi V$, where k_{12} contains all geometric factors pertaining to the coils, χ is the magnetic susceptibility, and V is the sample volume. For an infinite plane [Fig. 3(a)], the magnetic field H is applied parallel to the N/S interface and $V=Sx_0$, in which case $M\sim\chi x_0$. For the cylindrical geometry [Fig. 3(b)],

$$x_0=r\left\{\left[1+\left(\frac{M(T)-M(T_c)}{M(T_c)}\right)\right]^{1/2}-1\right\}, \tag{36}$$

where r is the radius of the superconducting core. It is clear that the magnetic field H generated by the primary coil is parallel to the N/S interface in this case. The situation is less clearly defined for the geometry shown in the Fig. 3(c). We argue first of all that the two or three superconducting spot welds, although acting as independent sources of superconductivity, are sufficiently close together and cover a sufficient portion of the end of the sample that they collectively approximate a continuous disk which, on a dimensional scale comparable to ξ_N, approximates the planar geometry shown in Fig. 3(a). The matter of the orientation of the applied magnetic field with respect to the N/S interface needs further comment. The magnetic field applied by the primary coil is clearly perpendicular to the interface. The Al spot welds, considered as a disk, distort this applied field, however, and induce a component parallel to the interface. Although we could not model this effect, we did measure the components of the magnetic field in the vicinity of a 7-cm-diam disk of Bi-Sr-Ca-Cu-O. We found that the component of the field parallel to the interface, $H_\parallel$, was roughly uniform for a given distance from the interface, that it was proportional to the applied field, and that it decreased as the distance from the interface. Thus, taking all of these considerations into account, we take $\delta M\sim\chi x_0$ for the geometry shown in Fig. 3(c) and $H_\parallel\alpha H$.

IV. RESULTS AND DISCUSSION

A. Characteristics of the samples

The measured resistivities at $T=4.2$ K for most of the Be samples were 5×10^{-8} Ω cm, whereas typical values for the W samples were 1×10^{-9} Ω cm. Thus the Be samples were in the dirty limit, in which case, from Eq. (4), $\eta\sim T$. The W samples were in the clean limit where $\eta\sim$const. Also, over the temperature region used, at least for the Be and W samples, Eq. (35) reduced to Eq. (23) so that the latter was appropriate to use to fit the data. Equation (23) may be rewritten in a three-parameter form suitable for fitting to the data in the clean and dirty limits:

$$x_0=\frac{a}{\sqrt{|\tau|T^\delta}}\ln\left[\frac{b\Delta_b}{\sqrt{H_\infty^2+H_0^2}}\sqrt{|\tau|}\right]+c \tag{37a}$$

$$=\frac{a}{\sqrt{|\tau|T^\delta}}\left[\ln\left(\frac{b\Delta_b}{\sqrt{H_\infty^2+H_0^2}}\right)+\frac{1}{2}\ln|\tau|\right]+c \tag{37b}$$

$$\sim m_2+\frac{m_1}{\sqrt{T^\delta|T-T_{cN}|}}. \tag{37c}$$

Here $\delta=1$ applies to the dirty limit and $\delta=2$ to the clean limit.

B. Results for tungsten samples with Al spot welds

1. Temperature dependence of the diamagnetism

The proximity effect was studied in over 30 tungsten samples which were decorated by Al spot welds. Several of those were incorporated into SRM devices and are referred to by the serial number of the device; samples not so incorporated are designated by a letter. The tungsten samples used in the SRM devices came from two uniform batches of material. The only known difference between the two batches was that all the tungsten rods in the first had $T_{cN}=15.5$ mK, while all the rods in the second had $T_{cN}=14.0$ mK. In both cases, the batches consisted of several cylindrical rods 50 mm long and 1.4 mm in diameter. All of these rods were single crystals with the long axis parallel to within $\pm2°$ of the (110) crystalline orientation. The rods had been purified by electron beam zone refining, and consequently the material was quite pure: The RRR of two of the 50-mm-long rods was measured and found to be 8900 $\pm$900. We conclude on the basis of Eq. (7) that, even at the lowest temperatures, these samples may be considered to be in the clean limit. SRM samples were spark cut from the 50-mm-long rods to a length of 9.5 mm. Both ends were polished to remove the damage due to the cuts, and two or three spots of Al were welded to one end.

Sample A was made from the second batch of tungsten; it differed from the SRM samples in that it was cut much

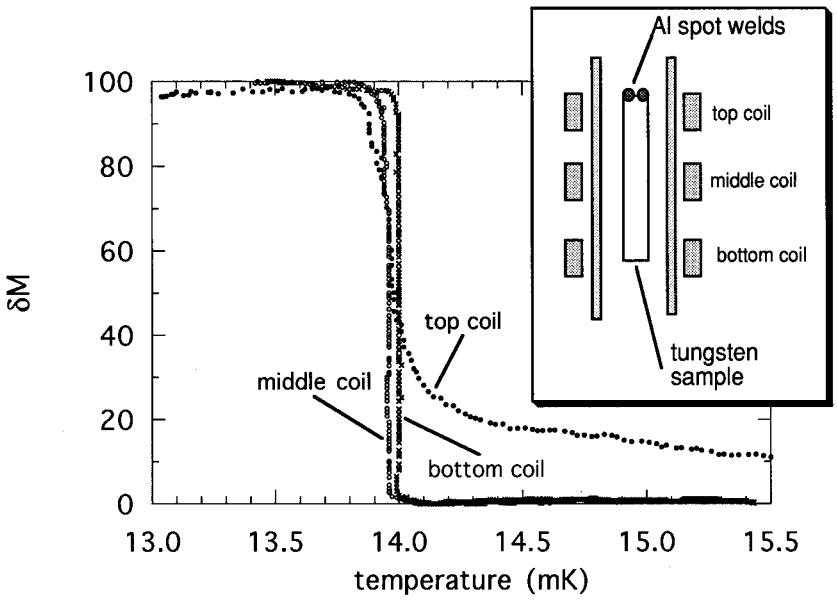

FIG. 4. Diamagnetism δM for three sections of sample WA as a function of temperature and at ambient magnetic field ($<0.1\,\mu$T). The rms value of the ac magnetic field applied to measure the diamagnetism was 0.047 μT. Inset: arrangement of the three coils relative to the sample. The proximity effect is quite apparent in the coil nearest to the two Al spot welds and is not discernible in the two coils farther away from the welds.

longer (31.8 mm) so that three parts of the sample (the end nearest the Al spot welds, the middle of the sample, and the end farthest from the spot welds) could be studied independently. Both ends were polished after cutting, and two spots of Al were welded to the upper end. Figure 4 shows the diamagnetism of this sample when it was measured in the nearly zero ambient magnetic field of the apparatus ($\sim 0.1\,\mu$T). The convention of arbitrarily normalizing the diamagnetism to $+100$ units for the perfect diamagnetism ($\chi = -1/4\pi$) below T_{cN} has been adopted throughout this article. Another convention used in the figures is to show only the warming transitions. The converse transitions were nearly identical to the S/N transitions *above* T_{cN}, but showed increasing hysteresis in larger applied magnetic fields *below* T_{cN}. Each transition was measured as the apparatus was warmed at a rate which was sufficiently slow (roughly 15 min) to guarantee that the sample was in thermal equilibrium with the calibrated resistance thermometer which defined the horizontal axis of the figure.

The coil shown in the inset to Fig. 4 which was nearest the Al spot welds exhibited a sizable proximity effect, whereas the coils at the middle and far end of the sample registered none. The equivalence of the curves for the middle and bottom ends of the sample rules out the possibility that the observed excess diamagnetism in the upper coil could be induced by the cutting or some other end effect. Further confirmation that the signal in the coil nearest the Al spot welds was due to the proximity effect comes from the fact that the extra diamagnetism was progressively suppressed by the application of a set of increasing, but small, magnetic fields. The magnetic field dependence of the diamagnetism at the end nearest the Al spot welds is not shown in this figure, but it behaved in the same way as will be shown below for similar W samples (e.g., samples 7, 44, and 77).

It could be argued that the excess diamagnetism observed above T_{cN} in the end of sample A was not due to the proximity effect, but arose instead from a broad superconductive transition due to a distributed alloy of Al and W formed at the juncture of the Al spot welds and the tungsten sample. It could be further argued that the suppression of the diamagnetism by weak magnetic fields was a manifestation of the putative weak superconductivity of the distributed Al-W alloy rather than a consequence of the proximity effect. The magnitude of the effect, however, argues cogently against the former interpretation and in favor of the latter. That is, just above T_{cN} in Fig. 4, the amplitude of the excess diamagnetism attains a value approximately one-half (50 units) of the full diamagnetic signal of the bulk tungsten. If we use the fact that the diamagnetic signal due to any superconductive transition is roughly proportional to the volume of the superconductor and we specify that the amplitude of the bulk W transition is, by convention, 100 units (100%), then we estimate that the maximum signal due to the proposed Al-W alloy would be at most 0.1 units, or 0.1%.[24] If we use a more accurate estimate, based not on the ratio of the volumes, but on coupling a diamagnetic W rod and a Al-W disk to a pickup coil, then we conclude that the maximum signal would be 0.2%.[25] In either case, these estimated effects are far too small to account for the observations.

We searched for the transition of the Al spot welds in the temperature region from 0.03 to 2 K and found a very small signal whose amplitude was 0.3% of the full W transition and which occurred over a temperature region of 0.13 K centered at a temperature of 0.55 K. Considering that the above estimate for the amplitude of the effect was made for a single spot weld, whereas the sample had two, the agreement between the predicted and measured amplitudes is excellent. In a separate experiment, we determined by a measurement of the resistance of the Al wire used for the spot welds that this material *before welding* had a superconductive transition extending from 1.00 to 1.14 K, which nearly coincides with the known T_c of pure Al (1.18 K).[26] Thus we conclude that the signal at 0.55 K was due to Al which had been degraded during formation of the spot welds.

All the tungsten samples with Al spot welds showed the influence of the proximity effect. The extent of the variation in the proximity effect observed among the samples is illustrated in Fig. 5, where the diamagnetism of four SRM W samples (7, 44, 77, and 88) just above their superconductive transitions are compared in the same ambient magnetic field ($\sim 0.1\,\mu$T). The three-parameter equation (37c) was least-squares fitted to these data, and the results are shown as solid

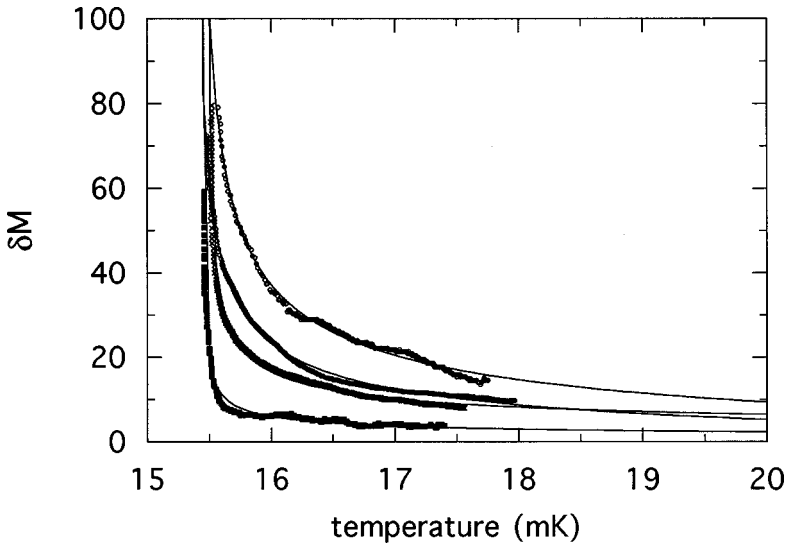

FIG. 5. Comparison of the diamagnetism δM of several W samples in ambient magnetic field ($<0.1\ \mu$T): reading from bottom to top, samples 88, 7, 44, and 77. The fitted values for m_1 obtained using Eq. (37c) were 15.9 ± 0.1, 41.4 ± 0.8, 83.4 ± 0.5, and 126 ± 1.6, respectively. The fitted values of T_{cN} were 15.452 ± 0.0001, 15.487 ± 0.0009, 15.393 ± 0.0009, and 15.409 ± 0.004 mK, respectively.

lines in the same figure. Equation (37c) contains the product of two separate functions of temperature: a strong singularity at T_{cN} and the comparatively weak factor T^{δ} which distinguishes the clean and dirty limits. The former was so dominant that the fits were insensitive to the latter, thus rendering a determination of δ impossible. The four curves diverge at a nearly common value of T_{cN}: Fitted values for T_{cN} ranged only from 15.4 to 15.5 mK. The absolute value of the diamagnetism was not measured in these experiments, so that the fitted value of m_1 contained an arbitrary factor. Nevertheless, the relative magnitude of the diamagnetism among the samples could be compared and it varied markedly. The samples are easily ranked in ascending order of the proximity effect (88, 7, 44, and 77) by inspection of Fig. 5. The values of m_1 (arbitrary units) determined from fitting Eq. (37c) to these data are 15.9 ± 0.1, 41.4 ± 0.8, 83.4 ± 0.5, and 126 ± 1.6 for samples 88, 7, 44, and 77, respectively. Some of the variation in this fitted coefficient may be due to the fact that the residual magnetic field was not controlled to better than 0.1 μT. Further differences in m_1 are presumably due to variation in the quality of the interface at the Al spot welds and/or to variation in T_{cS}. Put in terms of the model, both effects give rise to differences in Δ_b which influence the magnitude of the diamagnetism [see, for example, Eq. (23) or (37b)].

The diamagnetism as a function of magnetic field and temperature for three tungsten samples (77, 7, and 44) is shown separately in Figs. 6, 7, and 8. The curves exhibit several common features: For each sample and at a fixed magnetic field, the diamagnetism was found to increase gradually as the temperature was lowered until the bulk $T_{cN}(H)$ of W was approached, at which point the diamagne-

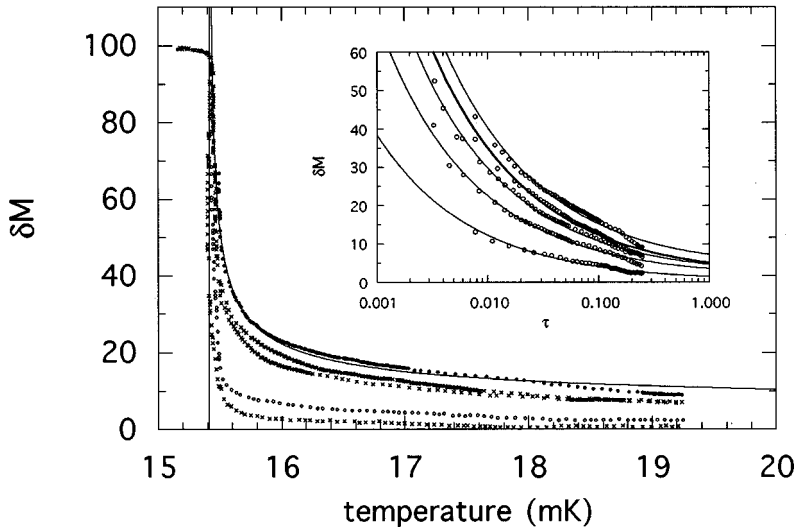

FIG. 6. Diamagnetism δM of sample W77 as a function of temperature at applied magnetic fields (proceeding bottom to top) of 3.0, 1.0, 0.6, 0.2, and 0 μT. The rms value of the ac magnetic field applied to measure the diamagnetism was 0.047 μT. The data are shown as points whereas a fit of Eq. (37c) to the data for $H=0$ (only one fit is shown for clarity) is shown as the solid line. Note the divergence in the fitted curve at $T_{cN}=15.436$ mK. For $H=3.0\ \mu$T the proximity effect had almost vanished, leaving the residual transition width of the bulk tungsten sample. Inset: the diamagnetism as a function of $\tau=(T-T_{cN})/T_{cN}$, where $T_{cN}(H)$ was obtained as one of the three fitted parameters. Reading from bottom to top, the value of the magnetic field for these curves was 2.0, 1.0, 0.6, 0.2, and 0 μT, respectively. Fits of Eq. (37c) to these data are shown as solid lines.

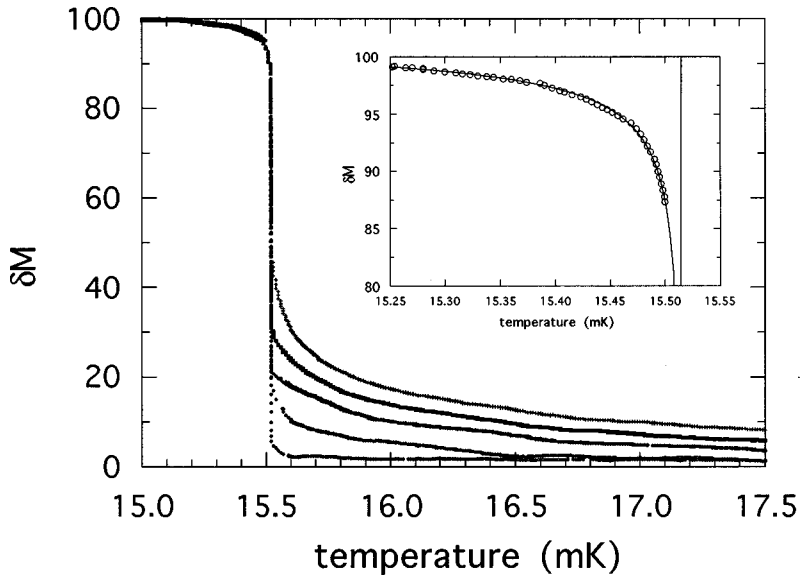

FIG. 7. Diamagnetism δM of sample W7 as a function of temperature at magnetic fields (proceeding bottom to top) of 2.0, 1.0, 0.4, 0.2, and 0 μT. The rms value of the ac magnetic field applied to measure the diamagnetism was 0.047 μT. The temperature scale for each curve has been shifted by the fitted value of $T_{cN}(H)$ to contrast the field-independent diamagnetism below T_{cN} (the residual width of the bulk transition) from the magnetic-field-dependent part above T_{cN} due to the proximity effect. From this plot it may be seen that for $H=0$ the proximity effect contributes an additional 45% to the diamagnetism. Similarly, the contributions are 38%, 20%, and 15% for $H=0.2$, 0.4, and 1.0 μT, respectively. The signal due to the proximity effect has practically vanished for $H=2.0$ μT. Inset: fit of the diamagnetism below T_{cN} to the temperature dependence of the penetration depth, $\lambda^{-2}(T)=\lambda_0^{-2}[1-t^4]$.

tism rapidly reached the full diamagnetism of bulk, superconducting tungsten. Two effects were always observed in an applied magnetic field: The proximity effect above T_{cN} gradually disappeared, and the bulk superconductive transition of the sample decreased in accordance with the expected BCS prediction.

In addition to the common features described above, each of these figures illustrates a different point about the proximity effect.

In Fig. 6 the data points for W77 are shown. A fit of Eq. (37c) above T_{cN} for the data at $H=0$ is displayed as the solid line. The divergence in the fit at $T_{cN}=15.436$ mK is clearly seen. Values for $T_{cN}(H)$ and thus τ were calculated for each value of magnetic field and the results replotted in the inset. The latter curves illustrate how close to T_{cN} the diamagnetism was measured. The solid curves drawn through the $\delta M(\tau)$ data represent fits of Eq. (37c) with the fitting parameter T_{cN} removed, i.e., $\delta M(\tau)=a+b/\tau^{1/2}$.

In Fig. 7 the transition from the bulk diamagnetic signal below T_{cN} to the proximity effect above T_{cN} was more clearly demonstrated for sample W7. The series of curves was constructed by replotting each transition with the temperature axis of each curve shifted by the amount $\delta T=(T_{cN}-T)$. Here δT was calculated from the BCS equation for $H_c(T)$, i.e., $H=H_c(0)\{1-[(T_{cN}-\delta T)/T_{cN})]^2\}$. Near T_{cN}, $\delta T=-HT_{cN}/2H_c(0)$. In this figure the family of curves exhibited a common, field-independent shape (the residual, bulk transition) below a common temperature and a field-dependent diamagnetism (the proximity effect) above that temperature. Thus the excess diamagnetism was fitted

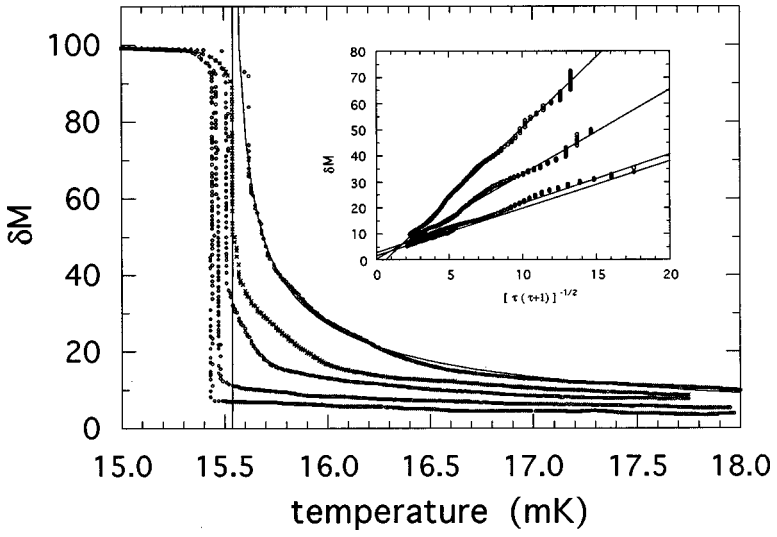

FIG. 8. Diamagnetism δM of sample W44 as a function of temperature at magnetic fields (proceeding left to right) of 2.0, 1.0, 0.4, 0.2, and 0 μT. The rms value of the ac magnetic field applied to measure the diamagnetism for all these curves was 0.047 μT. A fit of Eq. (37c) to the data for $H=0$ is shown as a solid line. Note the divergence at T_{cN}. Only one fit is shown for clarity. Inset: plot of the diamagnetism as a function of $[\tau(\tau+1)]^{-1/2}\sim\tau^{-1/2}$ for $H=1.0$, 0.4, 0.2, and 0 μT (proceeding bottom to top). The solid lines represent fits to these data of the equation $\delta M(\tau)=a+b\tau^{-1/2}$.

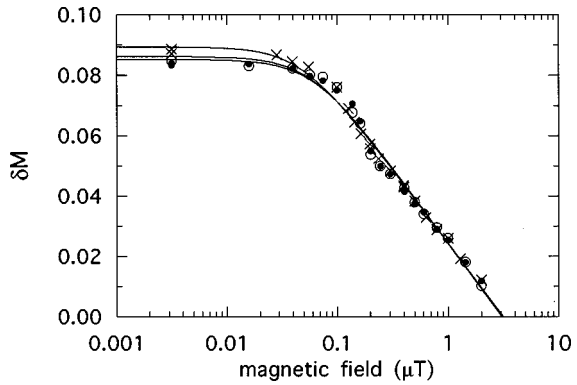

FIG. 9. Diamagnetism δM of sample W44 at a temperature of 15.90 mK as a function of magnetic field for three values of $H_{\rm rms}$ (open circles, $H=0.095\ \mu$T; solid circles, $H=0.143\ \mu$T; and crosses, $H=0.19\ \mu$T. Fits of Eq. (23) to the data are shown as solid lines. At low magnetic fields the diamagnetism was independent of field; at higher fields the diamagnetism decreased logarithmically. The values of H_0 obtained from Eq. (23) for $H_{\rm rms}$, 0.097, 0.143, and 0.19 μT, were, respectively, 0.059 ± 0.009, 0.063 ± 0.009, and $0.047\pm0.005\ \mu$T. Evidence such as this leads to the conclusion that H_0 was independent of $H_{\rm rms}$ to within experimental error.

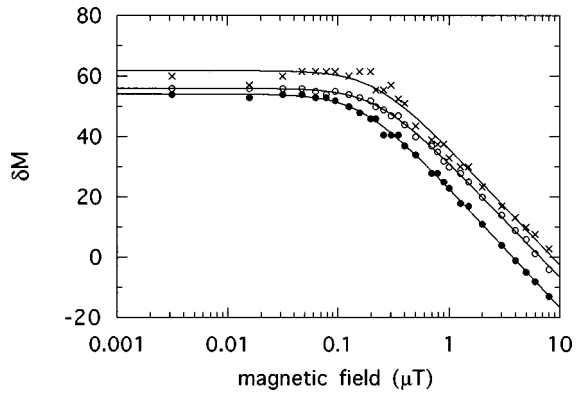

FIG. 10. Diamagnetism δM of sample W7 at three temperatures (solid circles, $T=15.88$ mK; open circles, $T=16.43$ mK; crosses, $T=17.24$ mK) as a function of magnetic field. All curves were taken with $H_{\rm rms}=0.107\ \mu$T. At low fields, the diamagnetism is independent of field; at moderate fields, it decreases logarithmically. The solid curves represent fits of Eq. (23). The values of H_0 obtained from the fits for $T=15.88$, 16.94, and 17.24 mK were, respectively, 0.15 ± 0.009, 0.177 ± 0.009, and $0.220\pm0.026\ \mu$T.

only in the temperature region above T_{cN} where it was clear that it was due exclusively to the proximity effect. For sample W7 where the proximity effect was moderately pronounced, the diamagnetism due to the proximity effect comprised 45% of the transition for $H=0$ and 38% for $H=0.2\ \mu$T, but it decreased to 20% when $H=0.4\ \mu$T, to 15% for $H=1.0\ \mu$T, and was too small to measure at 2.0 μT.

Since this sample (W7), as well as all the other W samples used in this study, was very pure and was a single crystal, it is possible that the temperature-dependent diamagnetism observed *below* T_{cN} is intrinsic and a manifestation of the temperature dependence of the penetration depth $\lambda(T)$. The diamagnetic signal for a pure material below T_c is proportional[27] to $[\delta-\lambda(T)]$, where δ is the skin depth. The temperature dependence of the penetration depth is given approximately by the two-fluid model result $\lambda^{-2}(T)=\lambda_0^{-2}/[1-t^4]$, where $t=T/T_{cN}$ and λ_0 is the penetration depth of the material at $T=0$. The diamagnetism due to the penetration effect is also expected to be independent of magnetic field. We found that the temperature dependence of the diamagnetism of the W samples below T_{cN} was quite consistent with that expected from the penetration depth for a pure material. For example, the inset to Fig. 7 shows the fit of the temperature dependence of the diamagnetism below T_{cN} using the two-fluid model. Furthermore, the signal was found to be independent of magnetic field below T_{cN}. Thus we conclude that the transition below T_{cN} represents that of pure tungsten. A more complete treatment of the diamagnetism below T_{cN} for the Be and W samples will be reported elsewhere.

According to the model presented herein, the temperature dependence of the diamagnetism above T_{cN} is dominated by the divergence, $\tau^{-1/2}$. To illustrate this feature more clearly, the diamagnetism for sample W44 is plotted versus $[\tau(\tau+1)]^{-1/2}\sim\tau^{-1/2}$ in the inset to Fig. 8. The straight lines drawn through the data are fits of $\delta M(\tau)=a+b\tau^{-1/2}$.

To our knowledge only one other group has studied the temperature dependence of the diamagnetism of the proximity effect for a N material with a finite T_{cN}. Deutscher and de Gennes[28] reported the $\delta M(T)$ curve for a $In_{1-x}Bi_x/Zn$ bilayer above the T_{cN} of the Zn (~0.92 K), while Deutscher, Hurault, and van Dalen[29] reported $\delta M(T)$ curves for another $In_{1-x}Bi_x/Zn$ bilayer as well as for Pb/Zn and Pb/Cd bilayers. We fitted these published data by Eq. (37c) and found implausible values for the fitted T_{cN} of Zn and Cd in the clean limit and insensitivity of the fit to the value of T_{cN} in the dirty limit. These ambiguities may be due to the fact that none of the curves contained points sufficiently close to the singularity at T_{cN} to clearly define it.

2. Magnetic field dependence of the diamagnetism

From such curves and others taken at much higher magnetic fields, the critical magnetic field curve $H_c(T)$ was also determined for several of the W samples. The results were fitted by the quadratic approximation to the BCS prediction: $H_c(T)=H_c(0)[1-(T/T_{cN})^2]$. For example, the data

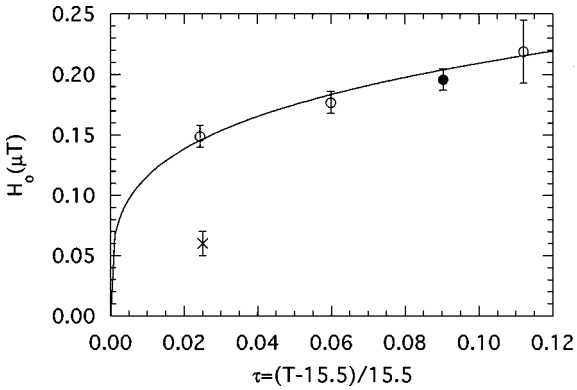

FIG. 11. H_0 vs τ for samples W7 (open circles), W44 ($\times$), and W77 (solid circle). The solid curve represents the fit of the form $H_0=a^*(\tau)^b$ to the data for sample W7, where $a=0.38\pm0.05\ \mu$T and $b=0.51\pm0.09$.

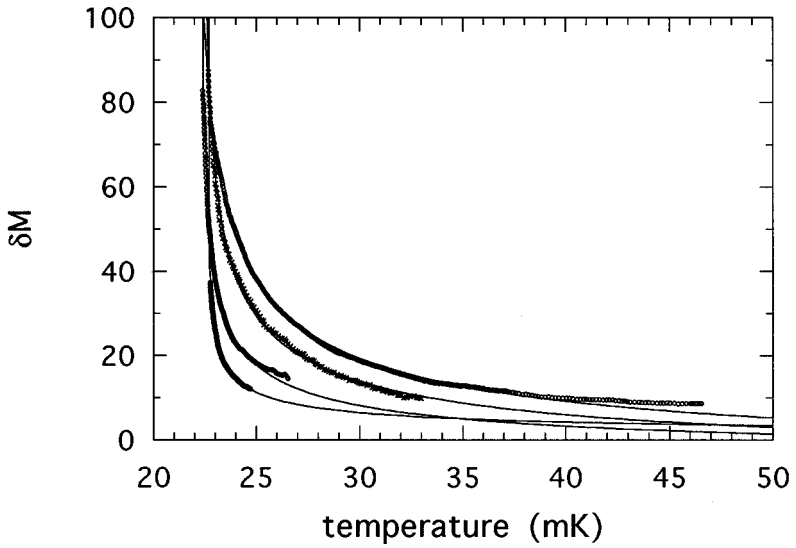

FIG. 12. Comparison of the diamagnetism δM of samples Be7, S-3, 92, and 44 (reading bottom to top) at ambient magnetic field ($<0.1\ \mu$T) as a function of temperature. The fitted values of the coefficient representing the strength of the proximity effect [parameter m_1 in Eq. (37c)] was 78.0 ± 0.28, 173 ± 1.1, 282 ± 2.9, and 395 ± 2.0 for samples 7, S-3, 92, and 44, respectively. The fitted values of T_{cN} were 22.56 ± 0.001, 21.94 ± 0.002, 22.24 ± 0.008, and 21.86 ± 0.011 mK, respectively. Note that the temperature scale for sample S-3 has been shifted by $+0.3$ mK for clarity.

taken for sample W7 yielded the fitted values $H_c(0)=0.12\pm0.01$ mT and $T_{cN}=15.485\pm0.011$ mK. These results are in good agreement with much more careful measurements conducted by Black, Johnson, and Wheatley[30] and by Triplett *et al.*[31] The samples were from different sources, but the RRR's were comparable. The former group found $H_c(0)=0.115\pm.001$ mT and $T_c=15.4\pm0.2$ mK, while the latter group found $H_c(0)=0.1237$ mT and $T_c=16.0$ mK.

The magnetic field dependence of the induced diamagnetism above T_{cN} was compared with the prediction of the model as well. The first procedure was to plot the fitted value of m_1 obtained for the three to five curves shown in Figs. 6–8 as a function of H. Such plots with so few points barely defined the functional form of $m_1(H)$, however. To establish a much better characterization of the phenomenon, a second procedure was employed in which the apparatus was stabilized at a temperature above $T_{cN}(H)$ and the output of the mutual inductance bridge was recorded at several values of H. Two examples for tungsten are shown in Figs. 9 and 10. In Fig. 9 the results for sample W44 are given when the temperature was maintained at 15.90 mK; one of three values of $H_{\rm rms}$ was chosen (0.097, 0.143, and 0.19 μT), and the magnetic field was varied. The curves for the two larger values of $H_{\rm rms}$ were scaled to the data for $H_{\rm rms}=0.097\ \mu$T. The shape of the $\delta M(H)$ curve is clearly independent of $H_{\rm rms}$. In Fig. 10 the results for sample W7 are given for three temperatures when $H_{\rm rms}$ was fixed at a value of 0.107 μT. Values of $\delta M(H)$ are shown in each figure for increasing and decreasing fields, and it is apparent that hysteresis, if present, was less than the resolution of the measurement ($\sim1\%$). For all curves the diamagnetism was constant at low magnetic fields, whereas it clearly decreased logarithmically at larger values. The data were fitted by Eq. (23), and the fits are shown as the solid curves in Figs. 9 and 10. We also verified another prediction of this equation: We reversed the dc current in the primary coil, thereby reversing the sign of H_∞. In accordance with Eq. (23), the data for the reversed field fell on the same curve as the data for the field in the original direction.

There could be three explanations for the origin of the field-independent diamagnetism at low magnetic fields which is displayed in Figs. 9 and 10. The first is that the transition at H_0 was the one predicted by Eq. (15). Another is that the logarithmic dependence of the diamagnetism at low magnetic fields was masked by an averaging effect due to the finite amplitude of the measuring magnetic field $H_{\rm rms}$.

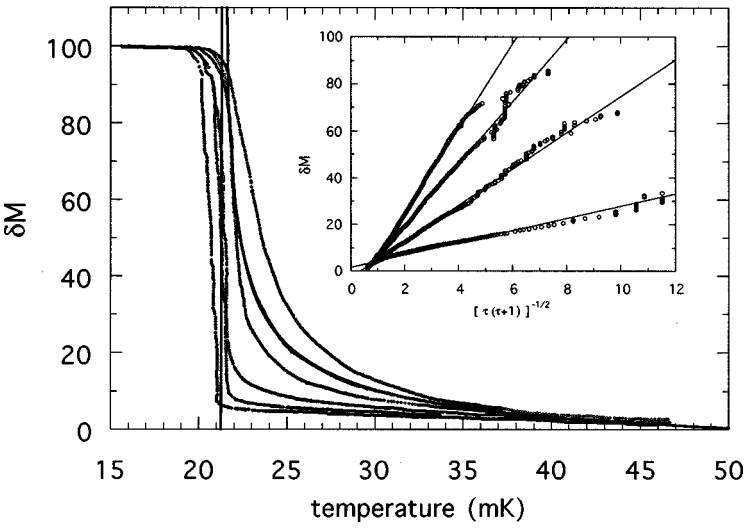

FIG. 13. Diamagnetism δM of sample Be44 as a function of temperature at magnetic fields (proceeding left to right) of 2.0, 1.0, 0.4, 0.2, 0.1, and 0 μT. The rms value of the ac magnetic field applied to measure the diamagnetism was 0.047 μT. Fits of Eq. (37c) to the curves for $H=0$, 0.1, 0.2, and 0.4 μT are shown as solid lines. Note the divergence of the fits at $T_{cN}(H)$, which were, respectively, 21.77, 21.67, 21.64, and 21.40 mK. For $H=2.0\ \mu$T, the proximity effect had vanished, leaving the residual transition width for this particular sample. Inset: the diamagnetism as a function of $\tau^{-1/2}$. The values of the applied magnetic field were (proceeding from left to right) 0, 0.1, 0.2, and 0.4 μT.

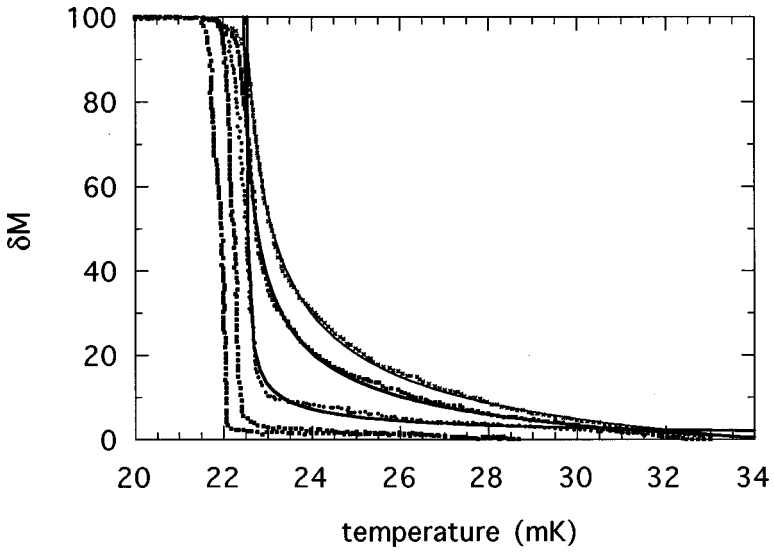

FIG. 14. Diamagnetism δM of sample Be92 as a function of temperature at magnetic fields (proceeding left to right) of 2.0, 1.0, 0.3, 0.1, and 0 μT. The rms value of the ac magnetic field applied to measure the diamagnetism was 0.047 μT. Fits of Eq. (37c) to the curves for $H=0$, 0.1, and 0.3 μT are shown as solid lines. Note the divergence of the fits at $T_{cN}(H)$ which were 22.30, 22.33, and 22.51 mK, respectively. For $H=1.0$ and 2.0 μT, the proximity effect had vanished, leaving the residual transition width of the bulk Be.

A third possibility is that the residual magnetic field H_r in the apparatus masked the logarithmic behavior at fields below that value. Deciding among the three effects should be easy since each one has a unique characteristic: The first is proportional to $(T\tau)$, the second depends on $H_{\rm rms}$, and the third is independent of everything. In Fig. 9 the fitted field was demonstrated to be independent of $H_{\rm rms}$, thereby eliminating the second hypothesis. Similar results were found for all the other W and Be samples, fully corroborating this conclusion. The values of H_0 obtained from the fits of Eq. (23) were comparable with the measured value of $H_r \sim 0.1$ μT (see Fig. 11), and it is difficult to to distinguish between these two possibilities. We display in Fig. 11 the measured values of H_0 as a function of τ for samples W7, W44, and W77. In the pure limit [$\eta = 7\zeta(3)/2\pi^3$] and also when $\Delta_b \gg k_B T$, Eq. (15) becomes

$$H_0 \sim \frac{12}{\sqrt{7\zeta(3)}} e^{-\gamma} T|\tau|^{1/2}\left(\frac{\phi_0 k_B \Delta_b}{\hbar^2 v_F^2}\right) = \frac{12}{\sqrt{7\zeta(3)}} e^{-\gamma} T_{cN}\left(\frac{\phi_0 k_B \Delta_b}{\hbar^2 v_F^2}\right)(\tau+1)|\tau|^{1/2}. \quad (38)$$

When the parameters for W (v_F and T_{cN}) and Al (Δ_b) are put into this equation, the equation becomes, for small values of τ, $H_0 \sim 0.24$ μT$\times|\tau|^{1/2}$. Accordingly, we fitted the equation $H_0 = a^*|\tau|^b$ to these data and obtained the values $a = 0.38 \pm 0.05$ μT and $b = 0.51 \pm 0.09$. Thus the temperature dependence of H_0 is accounted for by this model, whereas the magnitude is less so. We conclude that, although the temperature dependence favors the identification of the field as H_0 predicted by the model presented here, the magnitude is too close to H_r to decide the issue. Further experiments are anticipated in which better magnetic shielding will provide the condition $H_r \ll H_0$.

C. Results for beryllium samples with Al spot welds

The proximity effect was also studied in over 30 beryllium samples. Those incorporated into a SRM device are referred to with the serial number of the device, whereas samples not so incorporated are referred to by a letter. The beryllium samples incorporated into the SRM devices were made from the same batch of material which had been purified by a single vapor distillation, and thus they possess nearly identical properties, such as electrical resistivity and T_{cN}. The residual resistivity ratio (RRR) was 79 ± 1 for the

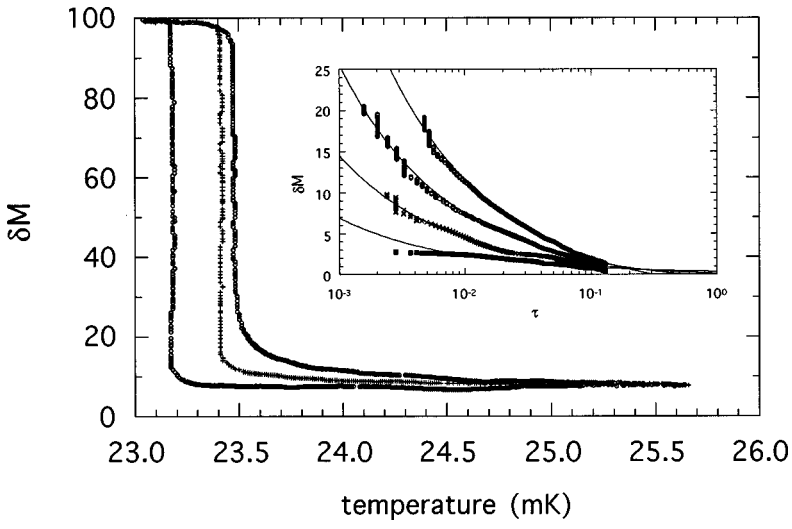

FIG. 15. Diamagnetism δM of sample Be-Fl as a function of temperature at magnetic fields (proceeding left to right) of 2.0, 0.2, and 0 μT. The rms value of the ac magnetic field applied to measure the diamagnetism was 0.047 μT. For $H=1.0$ and 2.0 μT, the proximity effect had vanished, leaving the residual transition width of the bulk Be. Inset: the diamagnetism as a function of $\tau=(T-T_{cN})/T_{cN}$, where $T_{cN}(H)$ was obtained as one of the three fitted parameters. The values of the applied magnetic field were (proceeding from bottom to top) 1.0, 0.4, 0.2, and 0 μT.

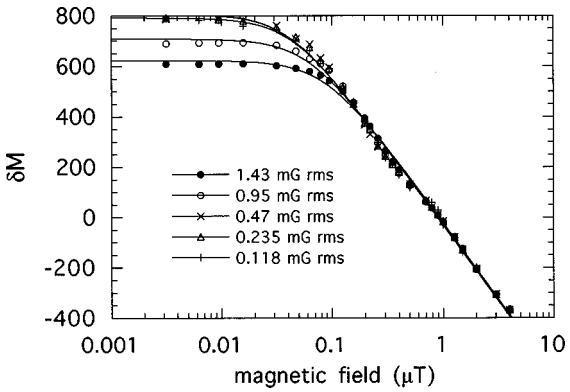

FIG. 16. Diamagnetism δM of sample Be44 at a fixed temperature (23.01 mK) as a function of magnetic field. The rms value of the measuring field was (proceeding from bottom to top) 1.90, 1.43, 1.43 (reverse direction), 0.095, 0.047, 0.0235, and 0.0118 μT. At low fields, the diamagnetism is independent of field; at moderate fields, it decreases logarithmically as expected from the model presented in this article. The solid curves represent fits of Eq. (23) to the data.

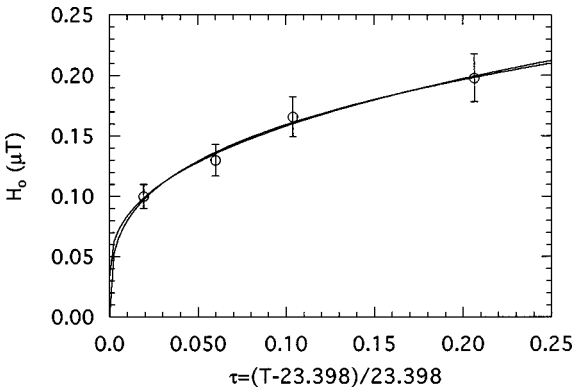

FIG. 17. H_0 vs τ for sample Be-Fl. The solid curve represents the fit of the form $H_0 = a^*(\tau)^b$ to the data, where $a = 0.32 \pm 0.02$ μT and $b = 0.30 \pm 0.03$.

SRM samples, indicating only moderate purity. T_{cN} values for the samples varied from 21.9 to 22.6 mK. The samples were irregularly shaped and were polycrystalline. For comparison, the proximity effect was also studied for one single crystal Be sample, Be-Fl, which had a residual resistivity ratio of 1000. We conclude on the basis of Eq. (7) that the Be samples with a RRR of 79 may be considered to be in the dirty limit, whereas the sample with a RRR=1000 is of intermediate purity.

The proximity effect was seen in all the Be samples studied. The diamagnetism of four SRM Be samples (labeled 7, S-3, 44, and 92) just above their superconductive transitions are compared in Fig. 12 in the same ambient magnetic field to illustrate the extent of the variation in the observed proximity effect. Least-squares fits of Eq. (37c) are shown as solid lines in the figure; the excellent fit of the data by this equation indicates strong evidence in support of the model used in this paper. The values for T_{cN} for these Be samples were similar and only varied from 21.86 to 22.56 mK. The *magnitude* of the diamagnetism, however, varied markedly for the four samples. The samples are easily ranked in ascending order (7, S-3, 92, and 44) by inspection of Fig. 12. The values of m_1 determined from fitting Eq. (37c) to these data are 78.0 ± 0.28, 173 ± 1.1, 282 ± 2.9, and 395 ± 2.0 for samples 7, S-3, 92, and 44, respectively. Such differences are presumably due to a variation in H_r and Δ_b.

The diamagnetism as a function of magnetic field and temperature for three samples is shown separately in Figs. 13–15. For each sample and at a fixed magnetic field, the diamagnetism was found to increase rapidly as the temperature was lowered until the bulk $T_{cN}(H)$ of Be was approached, at which point the diamagnetism reached full value $-1/4\pi$. Each sample had a residual superconductive transition width, which was manifest when the proximity effect was completely suppressed by a large magnetic field (2.0 μT for these samples). Owing to the moderate purity and polycrystalline quality of samples 7, 92, and 44, the residual superconductive transition width below T_{cN} varied considerably among the samples (roughly 70 μK for Be7, 400 μK for Be92, and 1.0 mK for Be44). By contrast, the intrinsic width of the single-crystal sample, Be-Fl, was very narrow (a few μK) and was consistent with the two-fluid model penetration effect. The transition from the bulk superconductivity of Be to the proximity effect was easily demonstrated by replotting the transitions (not shown) for each sample in which each curve at field H was shifted on the T axis by $T_{cN} - \delta$, where δ has been defined in the discussion for W7. The family of curves exhibited a common, field-independent shape (the bulk transition) below a common temperature and a field-dependent diamagnetism (the proximity effect) above that temperature. Thus the excess diamagnetism was fitted only in the temperature region above T_{cN} where it was clear that it was due solely to the proximity effect. Thus, for example, for sample 92, where the proximity effect was quite pronounced (Fig. 14), the diamagnetism due to the proximity effect comprised of 90% of the transition for $H=0$ and 80% for $H=0.1$ μT, but it decreased to 50% when $H=0.3$ μT and was too small to measure at 1.0 μT.

The temperature dependence of the diamagnetism as a function of magnetic field and the quality of the fits may be made clearer by plotting the diamagnetism as a function of τ. Such plots are shown for Be44 as an inset to Fig. 13 and for Be-Fl as an inset to Fig. 15.

The magnetic field dependence of the excess diamagnetism was compared with the prediction of the model as well. An example is shown in Fig. 16 for sample 44 where the temperature was controlled at 23.01 mK. Values of δM are shown for increasing and decreasing fields and it is apparent that hysteresis, if present, was less than the resolution of the measurement ($\sim 1\%$). The diamagnetism was studied for several values of $H_{\rm rms}$. For all curves the diamagnetism was constant at low magnetic fields, while it clearly decreased logarithmically at higher values. The data were fitted by [Eq. (23)], and the fits are shown as curves drawn through the data in Fig. 16, in which we have also modeled the effect of a finite value for $H_{\rm rms}$. When $H_{\rm rms}$ was below 0.047 μT, there was no effect on the diamagnetism, and the curves for $H_{\rm rms}=0.047$, 0.025, and 0.0118 μT were superimposed. H_0 was defined as a parameter determined from the fits. In order to compare the fitted values of H_0 with theory, we consider Eq. (15) in the dirty limit ($\eta = k_B T \tau_{\rm tr}/\hbar$) and also when $\Delta_b \gg k_B T$. Thus

$$H_0 \sim \frac{6}{\pi^3}\sqrt{7\zeta(3)}e^{-\gamma}|\tau|^{1/2}\left(\frac{\phi_0\Delta_b}{\hbar v_F^2\tau_{\rm tr}}\right). \quad (39)$$

When the parameters for Be (v_F, $\tau_{\rm tr}$, and T_{cN}) and Al (Δ_b) are put into this equation, the equation becomes $H_0 \sim 2.5\ \mu\mathrm{T}\times|\tau|^{1/2}$. Accordingly, we fitted the equation $H_0 = a^*|\tau|^b$ to these data (shown in Fig. 17) and obtained the values $a = 0.32 \pm 0.02\ \mu$T and $b = 0.30 \pm 0.03$. Neither the magnitude nor the temperature dependence of H_0 is well accounted for by this model, and the evidence favors the view that H_r is too close to H_0 to clearly distinguish them.

V. CONCLUSION

We have solved the Ginzburg-Landau equations for macroscopic samples where the normal metal has a nonzero superconductive transition temperature. We calculated the diamagnetism for the temperature region above T_{cN} and as a function of magnetic field. These calculations are compared with experimental measurements of the temperature (0.006–1 K) and magnetic field (10^{-9}–10^{-6} T) dependence of the diamagnetism for several samples of Be ($T_{cN} \sim 23$ mK) and W ($T_{cN} \sim 15.5$ mK) in contact with the superconductor Al ($T_{cS} = 1.18$ K). The agreement between the predictions and measurement is quite good for the temperature dependence and confirms the approach of using the Ginzburg-Landau model to calculate the proximity effect in macroscopic normal systems above their superconductive transitions. The magnetic field dependence needs more careful study.

ACKNOWLEDGMENTS

The experiments were carried out in a ^{3}He-^{4}He dilution refrigerator facility at the National Institute of Standards and Technology in Gaithersburg, MD. We are grateful for use of the facility during the measurements and for the support given by the staff from the Thermometry Group and the Fundamental Electrical Measurements Group at NIST. We also thank Marc P. Raphael (NRL) for measuring the magnetic field configuration surrounding a Bi-Sr-Ca-Cu-O disk.

*Retired.

[1] R. Holm and W. Meissner, Z. Phys. **74**, 715 (1932).

[2] T. Y. Hsiang and D. K. Finnemore, Phys. Rev. B **22**, 154 (1980), and references therein.

[3] R. W. Simon and P. M. Chaikin, Phys. Rev. **23**, 4463 (1981); **30**, 3750 (1984).

[4] J. H. Claassen, J. E. Evetts, R. E. Somekh, and Z. H. Barber, Phys. Rev. B **44**, 9605 (1991).

[5] G. Deutscher, J. Phys. Chem. Solids **28**, 741 (1967).

[6] Y. Oda, G. Fujii, and H. Nagano, J. Phys. (Paris), Colloq. **39**, C6-693 (1978); A. Sumiyama, Y. Oda, and H. Nagano, J. Phys. Soc. Jpn. **53**, 2449 (1984).

[7] Y. Oda, A. Sumiyama, and H. Nagano, Jpn. J. Appl. Phys., Part 1 **22**, 464 (1983).

[8] A. C. Mota, P. Visani, and A. Pollini, J. Low Temp. Phys. **76**, 465 (1989).

[9] Th. Bergmann, K. H. Kuhl, B. Schroder, M. Jutzler, and F. Pobell, J. Low Temp. Phys. **66**, 209 (1987).

[10] V. L. Ginzburg and L. D. Landau, Zh. Eksp. Teor. Fiz. **20**, 1064 (1950).

[11] P. G. de Gennes, Rev. Mod. Phys. **36**, 225 (1964); N. R. Werthamer, Phys. Rev. **132**, 2440 (1963).

[12] Groupe de Supraconductivite d'Orsay, in *Proceedings of the Sussex University Symposium*, edited by D. F. Brewer (North-Holland, Amsterdam, 1966).

[13] W. Belzig, C. Bruder, and Gerd Schon, Phys. Rev. B **53**, 5727 (1996).

[14] N. R. Werthamer, in *Superconductivity*, edited by R. D. Parks (Dekker, New York, 1969), p. 336, Eq. (4).

[15] P. G. de Gennes, A. Barone, and Yu. N. Ovchinnikov, Sov. Phys. JETP **50**, 735 (1979).

[16] L. G. Aslamasev, A. I. Larkin, and Yu. N. Ovchinnikov, Zh. Eksp. Teor. Fiz. **55**, 323 (1968).

[17] R. J. Soulen, Jr. and Deborah Van Vechten, Phys. Rev. B **36**, 239 (1987).

[18] Cryoperm 10, Vacuumschmelze, GMBH, D-6450 Hanau, Germany.

[19] We studied the residual magnetic field in the pair of shields at room temperature and found that it varied between the limits of $\pm 0.1\ \mu$T, when the inner shield was successively degaussed.

[20] W. E. Fogle, R. J. Soulen, Jr., and J. H. Colwell, in *Temperature, Its Measurement and Control in Science and Industry*, edited by J. F. Schooley (AIP, New York, 1992), Vol. 6, Pt. 1, pp. 91–96.

[21] R. J. Soulen, Jr. and R. B. Dove, *SRM 768 Superconductive fixed Point Device*, Natl. Bur. Stand. (U.S.) Spec. Publ. No. 260–62, (U.S. GPO, Washington, D.C., 1979).

[22] See, for example, Max Hansen and Kurt Anderko, *Constitution of Binary Alloys* (McGraw-Hill, New York, 1958), pp. 73 and 147.

[23] L. Hartshorn, J. Sci. Instrum. **2**, 145 (1924).

[24] The bulk, cylindrical W sample had a diameter $d = 0.14$ cm and was 0.9 cm long. We assume that the AlW alloy is a circular disk with the same diameter as the Al spot weld (0.025 cm) which is 0.025 cm deep. The ratio of the volumes is thus 8.4×10^{-4}.

[25] A diamagnetic W rod with radius a couples a magnetic flux Φ to a pickup coil of radius R by the expression, $\Phi = \pi a^2 H/4$, where H is the applied magnetic field. The analogous expression for a diamagnetic disk of radius r is $\Phi = 2r^3 H/R$. The ratio of the signals is thus $r^3/Ra^2 \sim 2\times 10^{-3}$.

[26] B. W. Roberts, J. Phys. Chem. Ref. Data **5**, 581 (1976).

[27] William D. Gregory, Phys. Rev. **165**, 556 (1968).

[28] G. Deutscher and P. G. deGennes, in *Superconductivity*, edited by R. D. Parks (Dekker, New York, 1969), Chap. 17, Fig. 6.

[29] G. Deutscher, J. P. Hurault, and P. A. van Dalen, J. Phys. Chem. Solids **30**, 509 (1969).

[30] W. C. Black, R. T. Johnson, and J. C. Wheatley, J. Low Temp. Phys. **1**, 641 (1969).

[31] B. B. Triplett, N. E. Phillips, T. L. Thorp, D. A. Shirley, and W. D. Brewer, J. Low Temp. Phys. **12**, 499 (1973).